Low-temperature photoluminescence studies of chemical-vapor-deposition-grown 3C-SiC on Si

W. J. Choyke, Z. C. Feng, and J. A. Powell

Citation: Journal of Applied Physics **64**, 3163 (1988); doi: 10.1063/1.341532
View online: http://dx.doi.org/10.1063/1.341532
View Table of Contents: http://scitation.aip.org/content/aip/journal/jap/64/6?ver=pdfcov
Published by the AIP Publishing

Low-temperature photoluminescence studies of chemical-vapor-deposition-grown 3C-SiC on Si

W. J. Choyke
Department of Physics and Astronomy, University of Pittsburgh, Pittsburgh, Pennsylvania 15260 and Westinghouse Research and Development Center, Pittsburgh, Pennsylvania 15235

Z. C. Feng[a)]
Department of Physics and Astronomy, University of Pittsburgh, Pittsburgh, Pennsylvania 15260

J. A. Powell
NASA Lewis Research Center, Cleveland, Ohio 44135

(Received 8 April 1988; accepted for publication 7 June 1988)

26 cubic SiC (3C-Sic) films grown on (100) Si by way of chemical vapor deposition (CVD) with SiC film thicknesses ranging from 600 Å to 25 μm have been studied by photoluminescence at 2 K. The "defect-related" W band near 2.15 eV appears in very thin-film samples. The G band near 1.90–1.92 eV and its phonon side bands G_1 and G_2 are believed to be related to dislocations and extended defects. The ratio ρ of the intensities of the G band and the strongest nitrogen-bound exciton (N-BE) TO(X) line may be used as a figure of merit for crystalline perfection in CVD 3C-SiC films. General formulas for the band-gap shift due to an axial stress, including three special cases—hydrostatic pressure and uniaxial and biaxial stress—are derived and applied to the CVD 3C-SiC/Si system. An experimental relationship of stress in these epitaxial films of 3C-SiC as a function of depth is obtained. It is shown that a 1–3 μm transition layer greatly reduces the interface misfit strain. For films thicker than 3 μm the film stress decreases slightly with increase of film thickness. The effects of biaxial stress on the relative intensities of N-BE lines are experimentally studied. It is reported that biaxial stress in the SiC/Si system depresses the intensity of the no-phonon line as well as the TA, LA, and LO phonon transitions of the N-BE spectrum.

I. INTRODUCTION

Cubic silicon carbide (3C-SiC) is a promising material for electronic and optical devices under severe environments, such as high temperature and high radiation flux. Its large energy gap, high electric breakdown field, high saturation drift velocity, moderately high electron mobility, temperature stability, and chemical inertness[1,2] lead to its desirable properties. However, crystals of cubic SiC obtained previously by the Lely process[3] were of relatively modest size and irregular shapes difficult to process for modern electronic applications. In recent years, interest in SiC has been renewed due to the successful epitaxial growth of 3C-SiC films on Si substrates by way of chemical vapor deposition (CVD).[4–7] It is necessary for the growth of single crystals of 3C-SiC on (100) Si to introduce simple hydrocarbons at room temperature, ramp the temperature to the growth temperature, and then continue the CVD deposition.[1,4] This process gives rise to a so-called "buffer layer"[1,4] or transition layer which accommodates the lattice mismatch by several, as yet ill defined, mechanisms. Although a large mismatch of about 20% in lattice constants between Si [5.430 Å at room temperature (RT)] and 3C-SiC (4.359 Å at (RT)] exists,[8] our Raman scattering studies[9,10] have shown that only 0.1%–0.2% strain exists near the surface regions in these CVD 3C films. This implies that linear elastic theory may be applied to these CVD 3C-SiC films. In Ref. 10, we have given a theoretical treatment for the Raman frequency shifts of a general heterostructure and applied it to the CVD SiC/Si system. Now we examine, first theoretically, the energy band-gap shifts under a generalized axial stress, which includes the case of hydrostatic pressure and uniaxial and biaxial stress. Then, we discuss the observed PL line shifts in CVD 3C-SiC due to the removal of the Si substrate.

PL is a sensitive, nondestructive, and useful technique for the characterization and study of semiconductor materials. A great deal of information about energy-band structure, impurities, structural defects, stresses, and strains may be obtained from PL measurements. The experimental setup for our PL measurements is described in Sec. III. The samples in this study were grown at the NASA Lewis Recearch Center, Cleveland, Ohio, by means of chemical vapor deposition (CVD).

A series of CVD 3C-SiC/Si PL spectra is shown in Sec. IV and discussed in Sec. V. Some free 3C-SiC films where the Si substrate has been removed, show PL spectra very much like those from high-quality bulk cubic SiC crystals. Attesting to the high quality of these films, we have seen for the first time three-phonon replicas due to the nitrogen-bound excitons (N-BE). Transmission electron microscopy (TEM) studies of CVD 3C-SiC/Si have shown that a high density of dislocations, stacking faults, twins, and microcrackings exist in the SiC films near the SiC/Si interface.[11–13] These interface misfit dislocations and defects act to relieve the stress in the films and also affect the PL spectra. The ration ρ of the line intensities of the defect-related band at 1.90–1.92 eV and the TO(X) replica of the N-BE line is a

[a)] Present address: Department of Physics, Emory University, Atlanta, GA 30322.

 0021-8979/88/183163-13$02.40

very rough measure of the quality of CVD 3C-SiC films. With an increase of SiC film thickness d_{SiC}, ρ decreases and saturates after $d_{SiC} > 15$ μm. Some additional PL spectral features are also reported.

II. THEORY

The effect of stain or stress on energy bands is described by the strain-orbit Hamiltonian and deformation potential coefficients.[14–18] For valence bands with p-like states and Γ_{25} symmetry (diamond) or Γ_{15} symmetry (zinc blende) near $\mathbf{k}=0$, i.e., the BZ center or Γ point, the Hamiltonian[14,16–18] is

$$H_\epsilon = -a(\epsilon_{xx}+\epsilon_{yy}+\epsilon_{zz}) - 3b\left[\left(L_x^2-\tfrac{1}{3}L^2\right)\epsilon_{xx}+\text{c.p.}\right] - (\sqrt{3}/6)d\left(\{L_x L_y\}\epsilon_{xy}+\text{c.p.}\right), \quad (1)$$

where ϵ_{ij} $(i,j=x,y,a)$ denotes the components of the strain tensor, L_i is the angular momentum operator, $\{L_x L_y\}=\frac{1}{2}(L_xL_y+L_yL_x)$, c.p. means the cyclic permutation of x, y and z, a is the hydrostatic pressure-deformation potential, and b and d are the uniaxial-deformation potentials appropriate to strains of tetragonal and rhombohedral symmetries, respectively.[14,16,17] Values of a, b, and d are negative, as a tensile strain and stress is defined to be positive and thus for a compressive strain and stress a, b, and d are positive. In this study of cubic SiC we are dealing with the indirect transitions related to the bottom of the conduction band at the X point and the top of the valence band at the Γ point. Therefore the deformation potentials a, b, and d given here are those of the valence band at the Γ point with respect to the bottom of the conduction band at the X point.

Epitaxial or deposited growth of thin layer films on a thick substrate may lead to the introduction of layer stresses and strains due to the differences of lattice constants and thermal expansion coefficients. Normally, one assumes that the layer stress component in the direction perpendicular to the surface of the substrate is different from that parallel to the surface of the substrate and the films. In the parallel plane, the components of stress and strain may be regarded as being isotropic. Without shear stress components, the stress tensor, taken to be symmetric about the z axis, can be decomposed into a hydrostatic pressure and a uniaxial stress along z axis as follows:

$$\begin{vmatrix} X & 0 & 0 \\ 0 & X & 0 \\ 0 & 0 & Z \end{vmatrix} = \begin{vmatrix} X & 0 & 0 \\ 0 & X & 0 \\ 0 & 0 & X \end{vmatrix} + \begin{vmatrix} 0 & 0 & 0 \\ 0 & 0 & 0 \\ 0 & 0 & P \end{vmatrix}, \quad (2)$$

where $Z=X+P$. We have three important special cases for this generalized axial stress: hydrostatic pressure corresponding to $P=0$, uniaxial stress corresponding to $X=0$, and the so-called biaxial stress[19,20] corresponding to $X=-P$, which possesses equal and opposite magnitude of hydrostatic and uniaxial components. The strain components for a generalized axial stress are

$$\epsilon_{xy}=\epsilon_{xz}=\epsilon_{yz}=0,$$
$$\epsilon_{zz}=(S_{11}+2S_{12})X=S_{11}P=\epsilon_\perp, \quad (3)$$
$$\epsilon_{xx}=\epsilon_{yy}=(S_{11}+2S_{12})X+S_{12}P=\epsilon_\parallel,$$

where S_{11} and S_{12} are the elastic compliances of cubic crystals, $\epsilon_\parallel$ is called the in-plane strain, and $\epsilon_\perp$ is the normal strain. From Eqs. (1) and (3), we have

$$H_\epsilon = -\delta E_h - \tfrac{3}{2}\delta E_s\left(L_z^2-\tfrac{1}{3}L^2\right), \quad (4)$$

where

$$\delta E_s = 2b(S_{11}-S_{12})P,$$
$$\delta E_h = a(S_{11}+2S_{12})(3X+P), \quad (5)$$

or for stiffnesses instead of compliances,

$$\delta E_s = 2bP/(C_{11}-C_{12}),$$
$$\delta E_h = a(3X+P)/(C_{11}+2C_{12}). \quad (6)$$

Equation (4) is written in the same form as used by Pollak and Cardona[16] for the case of uniaxial stress while δE_S and δE_H in our expressions (5) and (6) are different from theirs in Ref. 16. It has been shown[16,18] that with spin-orbit splitting $\Delta_0 \gg \delta E_s$, the energy differences between the conduction and valence bands at $\mathbf{k}=0$ are given by

$$\Delta(E_c-E_{v1}) = -\tfrac{1}{3}\Delta_0+\delta E_h-\tfrac{1}{2}\delta E_s,$$
$$\Delta(E_c-E_{v2}) = -\tfrac{1}{3}\Delta_0+\delta E_h-\tfrac{1}{2}\delta E_s, \quad (7)$$
$$\Delta(E_c-E_{v3}) = +\tfrac{2}{3}\Delta_0+\delta E_h.$$

We note that δE_S, the splitting between the heavy-hole (v_1) and light-hole (v_2) bands, depends only on the uniaxial component P but not on the hydrotstatic component X. The heteroepitaxial growth or deposition of a thin film on a thick substrate, for most of cases, can be regarded as possessing a biaxial stress distribution inside the thin film[19,20] with a uniaxial stress component, $P=-X$. Therefore, a tensile (compressive) biaxial stress has the same effect on δE_s as a compressive (tensile) uniaxial stress. For a compressive uniaxial stress component or a tensile biaxial stress with $P<0$ and $\delta E_S>0$ due to $b<0$ and $(S_{11}-S_{12})>0$, we have the heavy-hole band higher than the light-hole band and the change of the energy gap is

$$\delta E_g = \delta E_h - (1/2)\delta E_s. \quad (8)$$

For a tensile uniaxial stress component or a compressive biaxial stress with $P>0$ and $\delta E_S<0$, we have the light-hole band higher than the heavy-hole band and the change of energy gap is

$$\delta E_g = \delta\epsilon_h + (1/2)\delta E_s. \quad (9)$$

We have summarized the detailed expressions for energy-gap changes due to various stress situations in terms of stress, or strain, using S_{ij} or C_{ij}, in Table I. The changes are also shown schematically in Fig. 1. More details about Table I and Fig. 1 are given in Ref. 21.

III. EXPERIMENT

Experimental samples were grown at the NASA Lewis Research Center by means of chemical vapor deposition (CVD). Sample parameters are given in Table II. By use of a HF/HNO_3 1;1 etch solution, the Si substrates of a number of samples were etched away completely or partly leaving either an unsupported thin film of 3C-SiC or a window of 3C-SiC attached to a frame of (100) Si. In this manner it was possible to measure the PL spectra for 3C-SiC/Si or 3C-SiC free films from the front and back sides.

TABLE I. Band splitting and shift under axial stress.

	Generalized axial stress	Hydrostatic pressure	Uniaxial compression	Uniaxial tension	Biaxial compression	Biaxial tension
Stress	$\begin{vmatrix} X & 0 & 0 \\ 0 & X & 0 \\ 0 & 0 & X+P \end{vmatrix}$	$\begin{vmatrix} X & 0 & 0 \\ 0 & X & 0 \\ 0 & 0 & X \end{vmatrix}$	$\begin{vmatrix} 0 & 0 & 0 \\ 0 & 0 & 0 \\ 0 & 0 & P \end{vmatrix}$ $P<0$	$P>0$	$\begin{vmatrix} X & 0 & 0 \\ 0 & X & 0 \\ 0 & 0 & 0 \end{vmatrix}$ $X<0$	$X>0$
Strain	$\epsilon_{xy}=\epsilon_{xz}=\epsilon_{yz}=0$ $\epsilon_{xx}=\epsilon_{yy}=(S_{11}+2S)X+S_{12}P$ $\epsilon_{zz}=(S_{11}+2S_{12})X+S_{11}P$	$\epsilon_{xy}=\epsilon_{xz}=\epsilon_{yz}=0$ $\epsilon_{xx}=\epsilon_{yy}=\epsilon_{zz}=-\epsilon$ $=(S_{11}+2S_{12})X=X/(C_{11}+2C_{12})$	$\epsilon_{xy}=\epsilon_{xz}=\epsilon_{yz}=0 \quad \epsilon_{xx}=\epsilon_{yy}=PS_{12}=-\epsilon$ $\epsilon_{zz}=PS_{11}=-\epsilon S_{11}/S_{12}=\epsilon(1+C_{11}/C_{12})$		$\epsilon_{xy}=\epsilon_{xz}=\epsilon_{yz}=0 \quad \epsilon_{xx}=\epsilon_{yy}=(S_{11}+S_{12})x=-\epsilon$ $\epsilon_{zz}=2S_{12}X=-\epsilon S_{12}/(S_{11}+S_{12})=\epsilon C_{12}/C_{11}$	
δE_c	$2bP(S_{11}-S_{12})=2bP/(C_{11}-C_{12})$	0	$2bP(S_{11}-S_{12})=2bP/(C_{11}-C_{12})>0$	<0	$-2bX(S_{11}-S_{12})$ $=-2bX/(C_{11}-C_{12}) \quad <0$	>0
δE_h	$a(3X+P)(S_{11}+2S_{12})$ $=a(3X+P)/(C_{11}+2C_{12})$	$3aX(S_{11}+2S_{12})=3aX/(C_{11}+2C_{12})$	$aP(S_{11}+2S_{12})=aP/(C_{11}+2C_{12})>0$	<0	$2aX(S_{11}+2S_{12})=2aX/(C_{11}+2C_{12})>0$	<0
ΔE_g	$\delta E_h \pm \delta E_c/2$	δE_h	$\Delta E_g(\text{hh})=\delta(E_c-E_{v1})=\delta E_h-\delta E_c/2$	$\Delta E_g(\text{lh})=\delta(E_c-E_{v2})=\delta E_h+\delta E_c/2$	$\Delta E_g(\text{lh})=\delta(E_c-E_{v2})=\delta E_h+\delta E_c/2$	$\Delta E_g(\text{hh})=\delta(E_c-E_{v1})=\delta E_h-\delta E_c/2$
in P, S_{ij}	$a(3X+P)(S_{11}+2S_{12})\pm bP(S_{11}-S_{12})$	$3aX(S_{11}+2S_{12})$	$P[a(S_{11}+2S_{12})-b(S_{11}-S_{12})]$	$P[a(S_{11}+2S_{12})+b(S_{11}-S_{12})]$	$X[2a(S_{11}+2S_{12})-b(S_{11}-S_{12})]$	$X[2a(S_{11}+2S_{12})+b(S_{11}-S_{12})]$
in P, C_{ij}	$a(3X+P)/(C_{11}+2C_{12})\pm bP/(C_{11}-C_{12})$	$3aX/(C_{11}+2C_{12})$	$P[a/(C_{11}+2C_{12})-b/(C_{11}-C_{12})]$	$P[a/(C_{11}+2C_{12})+b/(C_{11}-C_{12})]$	$X[2a/(C_{11}+2C_{12})-b/(C_{11}-C_{12})]$	$X[2a/(C_{11}+2C_{12})+b/(C_{11}-C_{12})]$
in ϵ, S_{ij}	($+$ for $P>0$ and lh)	$-3a\epsilon$	$\epsilon[-a(S_{11}+2S_{12})+b(S_{11}-S_{12})]/S_{12}$	$\epsilon[-a(S_{11}+2S_{12})-b(S_{11}-S_{12})]/S_{12}$	$\epsilon[-2a(S_{11}+2S_{12})+b(S_{11}-S_{12})]/(S_{11}+S_{12})$	$\epsilon[-2a(S_{11}+2S_{12})-b(S_{11}-S_{12})]/(S_{11}+S_{12})$
in ϵ, C_{ij}	($-$ for $P<0$ and hh)	$-3a\epsilon$	$\epsilon[a(C_{11}-C_{12})-b(C_{11}+2C_{12})]/C_{12}$	$\epsilon[a(C_{11}-C_{12})+b(C_{11}+2C_{12})]/C_{12}$	$\epsilon[-2a(C_{11}-C_{12})+b(C_{11}+2C_{12})]/C_{11}$	$\epsilon[-2a(C_{11}-C_{12})-b(C_{11}+2C_{12})]/C_{11}$

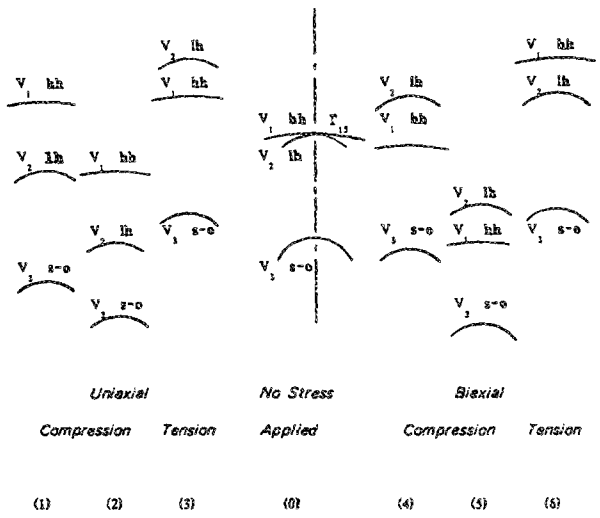

FIG. 1. Schematic of valence-band splittings and energy shifts under uniaxial and biaxial stresses.

3C-SiC has an energy gap of approximately 2.4 eV at helium temperature[22] and there is a large change in the absorption coefficient α and the penetration depth, $d_p = 1/\alpha$, as one goes from the band gap towards the vacuum ultraviolet. This is illustrated in Fig. 2. Actually, Fig. 2 is taken from room-temperature measurements and a small shift of about 25 meV towards higher energy would roughly give the abosrption at 2 K. For these experiments we use an Ar^+ laser with lines at 4880 and 4579 Å, a He-Cd laser with a line at 3250 Å, or a filtered high-pressure Hg lamp with a strong UV continuum and major lines at 3650, 4046, and 4350 Å. From Fig. 2, we find that the penetration depth d_p at room temperature in 3C-SiC is 83 μm at 2.6 eV (4767 Å), 48 μm at 2.7 eV (4591 Å), 5 μm at 3.4 eV (3650 Å), and $\sim$1.5 μm at 3.8 eV (3250 Å). The first two penetration depths are much larger than the 3C-SiC film thickness and thus we obtain only weak absorption in our SiC samples with an Ar^+ laser. For the Hg lines/ continuum and the He-Cd laser most of the energy is absorbed in our samples, making these sources more useful for the PL measurement. The high-pressure Hg lamp is very effective due to its high intensity and the ease of focusing but it limits the scan up to 6600 Å due to filtering difficulties for wavelengths beyond 6600 Å. The He-Cd laser is very useful for the near surface region of our CVD 3C-SiC films but, unfortunately, the output power from this laser is only 10 mW. When the He-Cd laser is used, the slits of the monochromator have to be widened, leading to lower resolution. As a compromise, both the 100-W high-pressure Hg lamp and the He-Cd laser are used.

The PL experimental arrangement is shown in Fig. 3. Samples were immersed in pumped liquid He at a temperature of <2 K to avoid noise generated by bubbles in normal liquid He and to get the sharpest possible line structure. By means of a special sample holder, samples were freely suspended in the liquid He to prevent additional stress due to mounting. The excitation light is focused on the sample surface to a spot with a 200–300 μm diameter when using He-Cd laser and a 0.5–1.0 mm diameter when using the Hg

TABLE II. Sample parameters and additional data.

Sample		CVD 3C-SiC (100)					(100) Si substrate		
No.	Size (mm^2)	d_{SiC} (μm)	Type	ρ (Ω cm)	n ($\times 10^{16}$ cm^{-3})	μ (cm^2 V^{-1} s^{-1})	d_{Si} (μm)	Type	ρ (Ω cm)
553	10×10	0.06					380	p	26
575	25× 7	0.2					380	p	26
227	25× 7	0.4						p	
481	25× 7	0.6	n					p	
98	24× 9	1	n					p	
537	14× 9	2	n				380	p	26
479	6× 8	3.2	n	1.5	3	150	382	p	25
476	7×11	4	n	1.0	4	170	382	p	25
480	8×10	4	n	0.5	7	190	382	p	25
482	6×10	4	n	1.3	3	160	382	p	25
488	6×10	4	n				382	p	25
461	14× 6	5	n	0.5	6	240	380	p	22
450	13× 7	6	n	0.2	10	310	500	p	22
408	12× 7	6	n	0.4	6	290	500	p	20
366	12× 7	7	n	0.05	100	140	380	p	47
629B	13×13	8.6	n	0.15	15	270	380	p	25
630	11× 7	9	n	0.3	6	350	380	p	25
631C	5× 7	10	n	0.14	20	250	380	p	25
484	11× 8	11	n				382	p	25
468	13× 9	13	n						
565	13× 8	15	n	0.07	30	300	380	p	25
99	6× 4	15	n		(same as TP099)		(Si substrate etched)		
440	10× 7	16	n	0.1			500	p	22
TP106	10× 9	17	n				500	p	
663C	6× 8	20	n	0.1			380	p	25
663A	6× 8	25	n	0.1			380	p	25

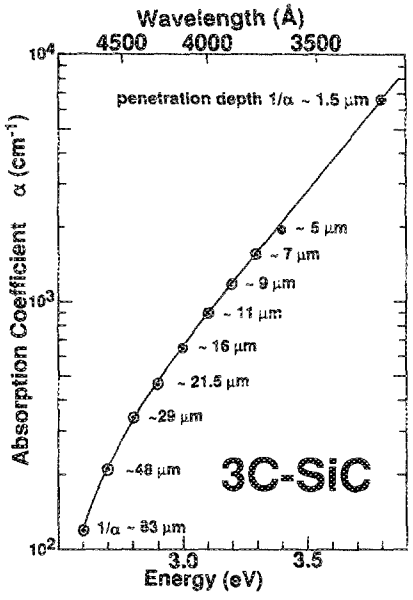

FIG. 2. Absorption coeficient α and penetration depth, $d_p = 1/\alpha$, of cubic SiC at 300 K.

lamp. In the latter arrangement we also inserted a Corning-9863 filter to attenuate radiation from 4500 to 6600 Å. The PL emission from the sample is focused onto the entrance slit of one section of a SPEX-1400 monochromator. For calibration, light from a standard line source is simultaneously focused onto the entrance slit together with the PL emision by means of a glass beam splitter. The optical signal dispersed by the SPEX-1400 is detected by a cooled RCA C31034 photomultiplier (PM) tube with a GaAs:Cs-O photocathode. The cooling substantially reduces the dark current noise in the PM tube. The output from the PM tube is sent to a PAR 128 lock-in amplifier and then fed into a microcomputer system. The LSI-11/03 microcomputer is used to control the scanning of the stepping motor, digitize the analog signals, and transmit the data to a Tandy-2000 microcomputer, which is used to record and store the experimental data, deal with the data processing, display simultaneously, and later plot out the PL spectra. The line resolution is 1 Å power 100 μm slit width. The signal sampling interval is usually much less than the line resolution to obtain highly resolved spectra.

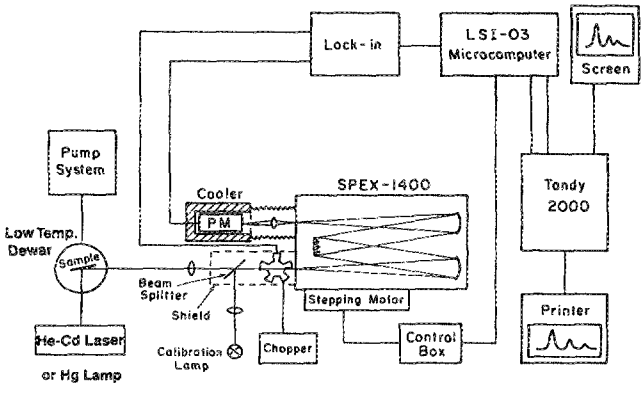

FIG. 3. Experimental arrangement for low-temperature photoluminescence measurement.

IV. RESULTS

A. PL spectra of CVD 3C-SiC films

Figure 4 shows a 2 K PL bound-excition (BE) spectrum including momentum conserving phonon replicas for one of our best 3C-SiC free films. The energy positions and assignments for spectralines are given in Tables III and IV. We find that this spectrum is very similar to that of reasonably pure bulk single-crystal 3C-SiC grown by the Lely technique.[22–24] The spectrum in Fig. 4 has a nitrogen-bound-exciton (N-BE) zero phonon line N_0, one-, two-, and three-phonon replicas, as well as a B-series BE line and its phonon replicas. The B lines may be due to an as yet unidentified impurity. Its no phonon line is displaced 7 meV to lower energy from the N-bound-exciton line. The BE lines in Fig. 4 have a full width at half maximum (FWHM) of less than 2 meV, which is comparable with the results in Refs. 22–24. The energy position of the N-BE lines and the deduced values of acoustic and optical phonon frequencies from our free film samples are nearly the same as those deduced from our purest bulk crystals grown by the Lely method and crystals grown from solution at SRI in the early 1960s.[22–24] Similar spectra have been reported by Feritas *et al.*[25–26] on crystal films grown at the Naval Research Laboratory and North Carolina State University, where only zero- and one-phonon lines of N-BE were assigned.

In order to get the best possible assignment for the multiple phonon combinations in Fig. 4, we made a thorough study of all possible phonon combinations with the energy difference from the no-phonon line N_0 up to 400 meV. The possible assignments for two-phonon combinations are listed in Table III. Those for three-phonon combinations are

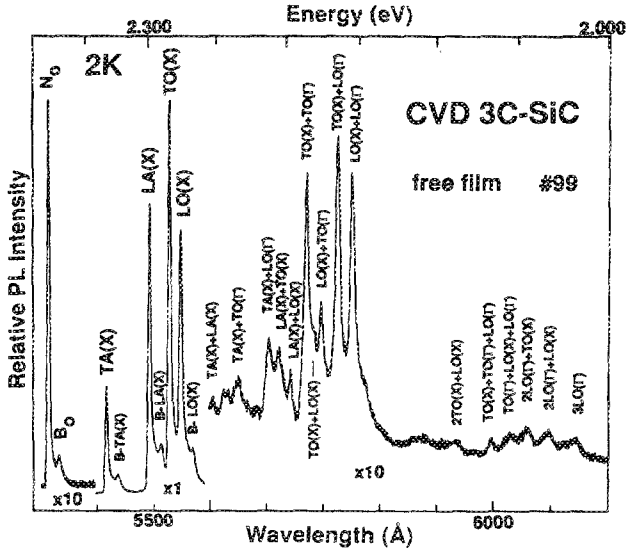

FIG. 4. Nitrogen-bound-exciton (N-BE) lines in a high-quality film of CVD 3C-SiC.

TABLE III. Zero-, one-, and two-phonon lines of N-BE for a 15-μm CVD 3C-SiC film (No. 99).

	Assignment	Energy (eV)	Shifts to N_0 (meV)
Zero phonon	0	2.3779	0
	B	2.3691	8.8
One phonon	TA(X)	2.3316	46.3
	B-TA(X)	2.3226	8.8 + 46.5
	LA(X)	2.2986	79.3
	B-LA(X)	2.2899	8.8 + 79.2
	TO(X)	2.2836	94.3
	LO(X)	2.2751	102.8
	B-LO(X)	2.2661	8.8 + 103.0
Two phonons	TA(X) + LA(X) (125.6 meV)	2.2506	127.3
		2.2432	134.7
	TA(X) + TO(X) (140.6)		
	TA(X) + TO(Γ) (145.0)	2.2326	145.3
	TA(X) + LO(Γ) (166.8)	2.2113	166.6
	LA(X) + TO(X) (173.6)	2.2050	172.9
	LA(X) + LO(X) (182.1)	2.1966	181.3
	TO(X) + TO(Γ) (193.0)	2.1851	192.8
	TO(X) + LO(X) (197.1)	2.1808	197.1
	LO(X) + TO(Γ) (201.5)	2.1755	202.4
	TO(X) + LO(Γ) (214.8)	2.1639	214.0
	LO(X) + LO(Γ) (223.3)	2.1549	223.0

listed in Table IV. Actually, higher-order phonon combinations could appear in the two- and three-phonon region. However, from Fig. 4, it is seen that the two-phonon lines are an order of magnitude weaker than the one-phonon lines and the third-order phonons are weaker again by another order of magnitude. Certainly the fourth-order and higher-order phonons are far too weak to appear in Fig. 4. The spectral features between 2.22 and 2.26 eV, only labeled with TA (X) + LA(X) and TA(X) + TO(Γ) in Fig. 4, do include the two-electron transitions of the N-BE in which the nitrogen donor is left in one of the excited states.[24] A higher-resolution spectrum would be required to carefully sort out the two-electron transitions from the two-phonon modes. Lines and bands in the energy region lower than 2 eV will be discussed later.

TABLE IV. Three-phonon replicas of N-BE (15-μm 3C-SiC free film sample No. 99).

Energy (eV)	Shifts from N_0 (meV)	Assignment	Phonons energy (meV)
2.0859	292.0	2TO(X) + LO(X)	291.4
		2TO(Γ) + TO(X)	291.7
2.0756	302.3	2LO(X) + TO(X)	299.9
		2TO(Γ) + LO(X)	300.2
2.0665	311.4	3LO(X)	308.4
		2TO(X) + LO(Γ)	309.1
		TO(X) + TO(Γ) + LO(Γ)	313.5
2.0556	322.3	TO(Γ) + LO(X) + LO(Γ)	322.0
2.0463	331.6	2LO(X) + LO(Γ)	326.1
		2LO(Γ) + TO(X)	335.1
2.0330	344.9	2LO(Γ) + LO(X)	343.8
2.0168	361.1	3LO(Γ)	361.5

B. PL spectra as a function of film thickness

Figure 5 shows 2 K PL spectra of 12 CVD 3C-SiC Si samples with 3C-SiC film thicknesses ranging from 600 Å to 17 μm. In Figs. 5(a)–5(f), we compare the PL spectra of six CVD 3C-SiC films on (100) Si substrates with a film thick-

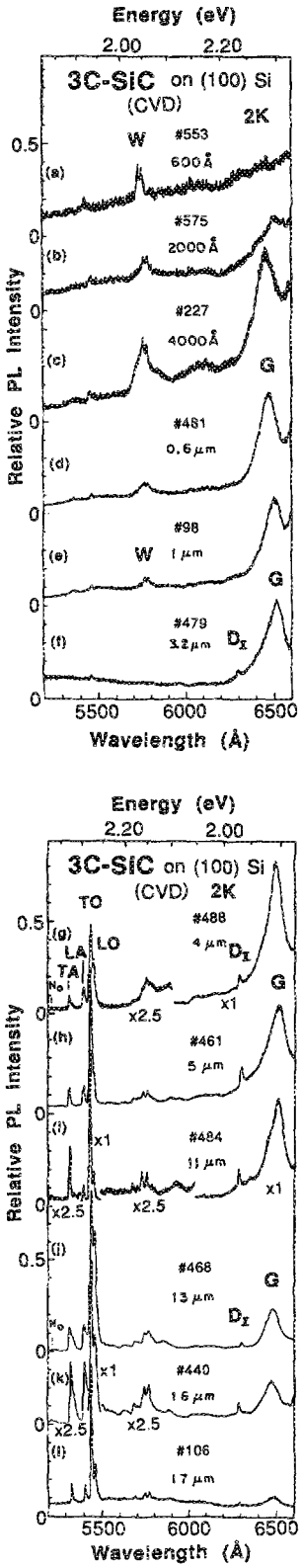

FIG. 5. 2 K photoluminescence spectra of CVD 3C-SiC/(100)Si with a film thickness d_{SiC} from 600 Å to 17 μm.

ness range of 600 Å–3.2 μm. The main features are as follows:

(1) A small indication of the main phonon replica of the N-BE center near 2.27 eV.

(2) A broad band at ~2.15 eV which dominates the spectrum of the thinnest sample (600 Å), but becomes less important with thicker films.

(3) A strong and broad band, named G, around 1.9–1.92 eV, is already apparent in the 2000-Å film and appears for almost all of the samples. At a film thickness of 3.2 μm we also see the appearance of the D_1 center no-phonon line at 1.972 eV.

In Figs. 5(g)–5(l), we compare six CVD 3C-SiC Si samples with film thicknesses ranging from 4 to 17 μm. Most striking is the development of the N-BE line structure and the virtual disappearance of the 2.15 eV band. More analysis and discussion will be given in Sec. V.

C. Line positions and ρ values with a variation of film thickness beyond 4 μm

For a number of CVD 3C-SiC/(100)Si samples with film thicknesses ranging from 4 μm to 25 μm, we hae carefully measured the PL spectral line positions obtained by means of two excitation sources, the Hg lamp and the He-Cd laser. Table V lists the corresponding data for the experimental samples, including the energy positions of the N-BE lines, the D_1 line, the broad band G near 1.90–1.92 eV, as well as the shift of N-BE TO(X) line relative to that for a stress-free sample shown in Fig. 4. The values of the ratio ρ are also listed in Tables V(a) and V(b) for two excitation sources.

D. Spectral comparison of the front and back of a "free" film of 3C-SiC

In order to study the structural difference between the near surface (front) and the near SiC/Si interface (back) region, we use the 3250-Å line of the He-Cd laser. The $1/\alpha$ point for the 3250-Å line in 3C-SiC at is about 1.5 μm. The PL spectra obtained from the front and back of sample No. 99 are shown in Fig. 6. The near surface region shows much stronger BE lines than the near interface region. The vacancy-related D_1 line,[27–28] the G, G_1, and G_2 bands, as well as a background below 1.95 eV are all relatively stronger in the interface layer than in the surface layer.

V. DISCUSSION

A. Effects of a tensile biaxial stress on BE transitions

The lattice constant of 3C-SiC at RT is 4.359 Å and is smaller than that of Si (5.430 Å at RT). The thermal expansion coefficient of 3C-SiC is slightly larger than that of Si.[8] Consequently, as an epitaxial 3C-SiC film is grown on a Si substrate by CVD, we have a tensile biaxial stress inside the SiC film. The Raman scattering studies[9,10,29,30] have shown that this tensile biaxial stress shifts the optical phonons of 3C-SiC to lower energies. According to the analysis in Sec. II, it also splits the $\mathbf{k} = 0$ (Γ point) degenerate valence band, puts the heavy-hole band on top, and consequently narrows

TABLE V. CVD sample data.

(a) Some CVD sample data under the excitation of the Hg lamp

Sample No.	d_{SiC} (μm)	N-BE line energy (eV) N_0	TA(X)	LA(X)	TO(X)	LO(X)	ΔE_{TO}[a] (meV)	D_1 (eV)	G (eV)	ρ
476	4		2.3256	2.2918	2.2760	2.2665	7.6	1.9713	1.9070	4.4
480	4		2.3251	2.2926	2.2765	2.2689	7.1	1.9713	1.9111	4.3
461	5		2.3241	2.2918	2.2765	2.2680	7.1	1.9726	1.9089	3.0
631C	10	2.3717	2.3256	2.2928	2.2774	2.2689	6.2	1.9719	1.9204	
468	13		2.3251	2.2920	2.2770	2.2689	6.6	1.9719	1.9157	0.25
565	15		2.3251	2.2918	2.2770	2.2684	6.6	1.9719	1.9204	0.25
440	16	2.3732	2.3251	2.2918	2.2770	2.2684	6.6	1.9719	1.9170	0.12
TP106	17		2.3252	2.2929	2.2775	2.2690	6.1	1.9716	1.1957	0.13
663A	25	2.3727	2.3256	2.2928	2.2779	2.2703	5.7	1.9716	1.9143	0.17
99[b]	15	2.3779	2.3316	2.2986	2.2836	2.2751	0	1.9726	1.9029	0.072

(b) Some CVD sample data under the excitation of the He-Cd laser

Sample No.	d_{SiC} (μm)	N-BE line (eV) N_0	TA(X)	LA(X)	TO(X)	LO(X)	ΔE_{TO} (meV)	D_1 (eV)	G (eV)	ρ
461	5		2.3246	2.2913	2.2765	2.2689	7.1	1.9717	1.9067	0.78
631C	10	2.3725	2.3254	2.2933	2.2775	2.2700	6.1	1.9723	1.9158	0.13
468	13	2.3725	2.3254	2.2919	2.2775	2.2694	6.1	1.9728	1.9167	0.09
565	15		2.3262	2.2933	2.2782	2.2700	5.4	1.9718	1.9196	0.16
440	16		2.3262	2.2940	2.2782	2.2700	5.4	1.9728	1.1982	0.11
663C	20		2.3269	2.2953	2.2789	2.2707	4.7	1.9733	1.9182	0.06

[a] ΔE_{TO} is taken with respect to the N-BE TO(X) position of No. 99.
[b] A free film as the standard.

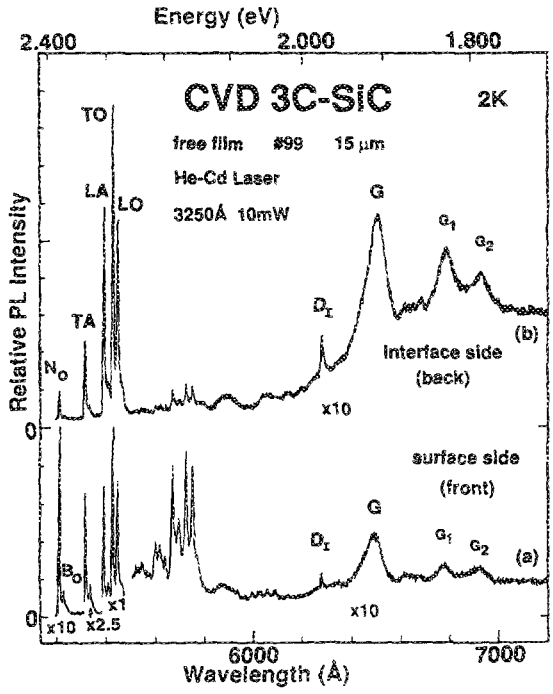

FIG. 6. 2 K photoluminescence spectra from both sides of a 15 μm CVD 3C-SiC film.

the energy-band gap. These splittings and shifts are shown schematically in Fig. 1. The band-gap change due to a tensile biaxial stress is calculated with the expression

$$\Delta E_g = X[2a(S_{11}+2S_{12}) + b(S_{11}-S_{12})] \qquad (10)$$

from Table I. Since $a<0$, $b<0$, and $X>0$ for a tensile stress, we have $\Delta E_g < 0$. Our PL measurements in Fig. 5 and Table V confirm this conclusion. The N-BE and phonon replicas from 3C-SiC/Si samples shift to lower energies by 4–7 meV in comparison with 3C-SiC free film in Fig. 5 and Table V. A preliminary version of these results has already been given by us earlier.[29] Furthermore, similar experiments also using a "frame geometry" for the unsupported 3C-SiC CVD film has been published by Freitas *et al.*[25,26] They found a qualitatively similar shift for the N-BE lines when comparing a film in the supported and unsupported mode. Because the 3C-SiC deformation potentials at $\mathbf{k}=0$ for the top valence band relative to the bottom of the conduction band, at the X point of the Brillouin zone, are not available, we are not able to use Eq. (10) to calculate the stress inside the 3C-SiC film on Si. However, we have available an estimate of the values of stress X from our Raman measurements and we observe line shifts presumably related to the band-gap shift ΔE_g from the PL measurement. This enables us to make a rough estimate of the range of the deformation potentials in 3C-SiC.

Let us consider sample No. TP106 with a d_{SiC} of 17 μm. The Raman measurements in Ref. 10 give an average stress inside the 3C-SiC/(100)Si film of $X=0.61$ GPa or 6.1×10^9 dyn/cm^2. As a consequence of the analysis in Ref. 10, we find that our best choice is to make use of the following compliances of 3C-SiC, namely, $C_{11}=5.4$ and $C_{12}=1.8\times10^{12}$ dyn/cm^2, which are obtained from the thermal conductivity measurements of Slack.[31] We have

$$S_{11}+2S_{12}=1/(C_{11}+2C_{12})=1.11\times10^{13}\ \text{cm}^2/\text{dyn},$$
$$S_{11}-S_{12}=1/(C_{11}-C_{12})=2.78\times10^{-13}\ \text{cm}^2/\text{dyn}. \qquad (11)$$

With $\Delta E_g=-6.2$ meV for sample No. TP106 and the above values, we have from Eq. (10)

$$2.2a+2.8b\sim-10\ \text{eV}, \qquad (12)$$

where the deformation potentials a and b are in units of eV.

Recall that the penetration depth of the light in 3C-SiC at 5145 Å, in the Raman experiments,[9] is at least 400 μm whereas for the 3250-Å and 3650-Å lines in the PL, the penetration is only 1.5 and 5 μm, respectively. We have measured the PL spectra for a number of samples by using a variety of different excitation sources and the corresponding line positions have already been listed in Tables V(a) and V(b). Figure 7 shows the shift of the TO(X) line of the N-BE from the line position of the stress-free sample No. 99. We can see that the TO(X) line of the N-BE spectrum shifts linearly with film thickness for both the He-Cd laser and the filtered Hg lamp. However, the slope of the data obtained with the He-Cd laser is steeper, as might be expected if there is a stress gradient within these films. Our Raman measurements using the 5145-Å line obtain an average stress value for the SiC films. The Raman shifts after removal of the Si substrates are only about 1–2 cm^{-1}, i.e., 0.25–0.5 Å or 0.12–0.25 meV. Contrast this with the exciton line shifts in PL measurements which are about 4–7 meV or 10–18 Å. This large difference between the Raman and PL measurements is due to the different mechanisms that are applicable. The Raman photon line shifts due to stress are connected with the changes in the first-order derivatives of the effective spring constants.[32] These changes are very small and lead to the small Raman line shifts that we observe. PL measurements directly detect the variation of the energy-band gap with the applied (built-in) stress. The band-gap change with lattice constant is a much larger effect than the perturbation in the

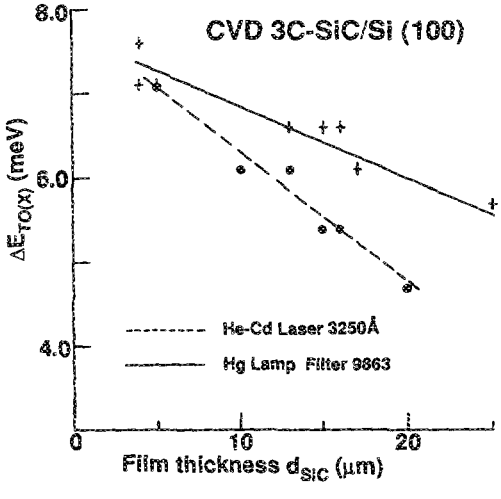

FIG. 7. TO(X) line shift as a function film thickness.

spring constants. Nevertheless, there are a number of conditions under which LT-PL cannot be applied whereas RT Raman measurements will give useful data. It is desirable to have both techniques in hand.

Figure 7 shows that with an increase of film thickness, the energy-band-gap shift ΔE_g of the SiC film decreases. According to Eq. (10) the biaxial stress (X) should then also decrease. The numerical rate of the increase of stress with depth may now be calculated. From Fig. 7, for the dashed line, measured under the excitation from the He-Cd laser, we have $\delta E_g/\delta d_{\rm SiC} = 0.162$ meV/μm and from Eqs. (10) and (11), we have $\delta E_g/\delta X = -10$ meV/GPa. Therefore,

$$\delta X/\delta d_{\rm SiC} = -0.0162\ \text{GPa}/\mu\text{m} \sim -0.02\ \text{GPa}/\mu\text{m}\ . \tag{13}$$

If we use the solid line in Fig. 7, obtained with Hg lamp excitation, we have $\delta E_g/\delta d_{\rm SiC} = 0.086$ meV/μm and

$$\delta X/\delta d_{\rm SiC} = -0.0086\ \text{GPa}/\mu\text{m} \sim -0.01\ \text{GPa}/\mu\text{m}\ . \tag{14}$$

The former is twice that of the latter. This difference might be explained by considering the different penetration depths of the He-Cd laser 3250-Å line and the filtered Hg lamp. The He-Cd 3250-Å line penetrates the near surface region only whereas the Hg lamp will excite all of the film including the SiC/Si interface region. This is the region of largest stress and will tend to dominate the measurement. The stress measured using the Hg lamp will therefore decrease slower with sample thickness than that using the He-Cd laser.

B. Influence of small spin-orbit splitting on the shift of the energy gap

In the discussion in Sec. II, there is a requirement that $\delta E_s \ll \Delta_0$, i.e., the spin-orbit splitting should be much larger than the splitting of the heavy- and light-hole bands due to stress. The spin-orbit splittings of Si, cubic SiC, and the uniaxial polytypes of SiC are 44, 10, and 7 meV,[33] respectively. For the case of Si, the requirement of $\delta E_s \ll \Delta_0$ is easily satisfied. But for CVD cubic SiC on Si, we observe bound-exciton (BE) line shifts from 4 to 7 meV due to the removal of the Si substrate. The condition that $\delta E_s \ll \Delta_0$ may not be satisfied. We will now discuss the case of small spin-orbit splitting on the energy-band shifts. From the strain-orbit Hamiltonian (4), Pollak and Cardona[16] have obtained the changes of the energy-band difference between the conduction and the heavy- and light-hole valence bands at $\mathbf{k} = 0$ without the limitation, $\delta E_s \ll \Delta_0$:

$$\Delta(E_c - E_{v1}) = \tfrac{1}{6}\Delta_0 + \delta E_h - \tfrac{1}{4}\delta E_s - \tfrac{1}{2}\left[\Delta_0^2 + \Delta_0 \delta E_s + \tfrac{9}{4}(\delta E_s)^2\right]^{1/2} \tag{15}$$

and

$$\Delta(E_c - E_{v2}) = -\tfrac{1}{3}\Delta_0 + \delta E_h + \tfrac{1}{2}\delta E\ . \tag{16}$$

From Eq. (16), the position of the light-hole band $v2$ is not affected by the relation between δE_s and Δ_0. In the case of uniaxial tension and biaxial compression, the light-hole band lies above the heavy-hole band and determines the band gap. The band gap, under these conditions, is not affected by a small spin-orbit splitting. While the position of the heavy-hole band $v1$ with respect to the bottom of the conduction band is changed as seen from Eq. (15). For $\delta E_s < \Delta_0$, keeping first and second-order terms in δE_s, we have the band-gap change due to stress

$$\Delta E_g = \Delta E_g(\text{hh}) = \delta(E_c - E_{v1}) = \delta E_h - \tfrac{1}{2}\delta E_s - \tfrac{1}{2}(\delta E_s)^2/\Delta_0 + \cdots\ , \tag{17}$$

The first and second term in Eq. (17) is the energy-gap change in Eq. (8) under the limitation of a large spin-orbit splitting. The third term in (17) represents an additional energy shift ΔE_g^* appearing for a small spin-orbit splitting where

$$\Delta E_g^* = -\tfrac{1}{2}(\delta E_s)^2/\Delta_0\ , \tag{18}$$

which further decreases the energy-band gap. For $\delta E_s > \Delta_0$, we have from (15)

$$\Delta E_g = \Delta E_g(\text{hh}) = \delta(E_c - E_{v1}) = \delta E_h - \tfrac{1}{2}\delta E_s - \tfrac{1}{2}\delta E_s - \tfrac{4}{27}(\Delta_0)^2/\delta E_s + \cdots\ . \tag{19}$$

Another additional term ΔE_g^{**} appears in (19) in comparison with (8)

$$\Delta E_g^{**} = -\tfrac{1}{2}\delta E_s - \tfrac{4}{27}(\Delta_0)^2/\delta E_s\ , \tag{20}$$

which makes the energy-band-gap decrease for $\delta E_s > 0$ and increase for $\delta E_s < 0$. For the case of CVD 3C-SiC/Si, we have a tensile biaxial stress and $\delta E_s > 0$ in the SiC film. The energy band gap becomes smaller due to a tensile biaxial stress under the approximation of a large spin-orbit splitting. From Eqs. (15)–(20), under the condition of a small spin-orbit splitting, we find a further decrease of ΔE_g^* given in (18) for the case of $\delta E_s < \Delta_0$ or by ΔE_g^{**} given in (20) for the case of $\delta E_s > \Delta_0$. Indeed, supposing that the maximum value of δE_s for CVD cubic SiC is 7 meV, we then have a further reduction of the energy band gap of

$$\Delta E_g^* = \tfrac{1}{2}(\delta E_s)^2/\Delta_0 \sim 2.5\ (\text{meV})\ . \tag{21}$$

This represents a *maximum* error of 30%. Our analysis given above and the schematic in Fig. 1 are qualitatively unchanged by this correction.

C. Crystallinity-dependent PL features and ρ value

TEM studies of CVD-grown 3C-SiC on (100) Si have shown that near the SiC/Si interface (within 2–3 μm), there exists a high density of defects[12] and the defect density decreases rapidly over a distance of 3–4 μm from the interface.[11] The main structural defects are misfit dislocations, stacking faults, and twins[11–13] as well as microcracking.[8] Our PL results are consistent with these TEM observations. In Figs. 5(a)–5(f), PL spectra of samples with $d_{\rm SiC}$ less than 3 μm show very weak BE emission and the dominant emission is a 2.15-eV band and the G band near 1.90–1.92 eV. The broad band near 2.15 eV is reminiscent of the W band seen in plastically deformed 6H-SiC near 2.7–2.8 eV (Ref. 34). To emphasize the similarity with the 6H-SiC 2.7–2.8-eV feature we also designate it as a W band. It dominates the spectrum of the thinnest sample with $d_{\rm SiC} = 600$ Å and gradually becomes less important with an increase of film thickness. For samples in Figs. 5(g)–15(l), with $d_{\rm SiC}$ larger than 4 μm, the

W band is much weaker than the two phonon replicas of the N-BE. It is reasonable to assume that the W band near 2.15 eV has a similar origin as the W band in 6H-SiC (Ref. 34) and is therefore due to heavy deformation in the near interface region. For $d_{SiC} > 3\,\mu$m, the W band appears occasionally in a few samples, which may mean that these samples have a thicker deformation region. For most of the samples with $d_{SiC} > 4\,\mu$m, the region beyond the transiton region has been shown[9,10] to possess a relatively small amount of strain on the order of 0.1%–0.2%. Therefore, the W band, which we presume to be related to deformation, is too weak to be seen beyond the transition region.

Furthermore, it should be pointed out that the energy region of the W band around 2.15 eV also slightly overlaps the energy region of the phonon sidebands of the D_{II} defect band reported previously in implanted cubic SiC crystals[28,35] and films.[26] It is natural to inquire whether the W band could be a broadened version of D_{II} or not. Our results, thus far, lead us to believe that the W band is not a broadened version of D_{II} for the following reasons. D_{II} features appear in ion-implanted samples and have been associated with carbon interstitials (pointlike) defects.[28,35] In none of our thicker ($d_{SiC} > 5\,\mu$m) unimplanted 3C-SiC film samples have we observed the appearance of the D_{II} band. The W band appears in thin SiC film samples where the dominant defects are dislocations and extended defects and these films are heavily deformed. We have no evidence, at present, that carbon interstitials are a dominant feature in our thin CVD SiC films.

The strong and broad band G around 1.90–1.92 eV appears for almost all of the samples. The D_I no-phonon line at 1.972 eV, which has been attributed to a divacancy related center, appears at film thicknesses greater than 3.2 μm. The D_I line and G band both sharpen as we go from 4 to 11 μm. We find an interesting variation of the relative intensities between the N-BE and the G band as we increase d_{SiC}. The strongest N-BE line [TO(X)], is weaker than the G band in 4 μm samples, while it is stronger than the G band in 5 and 11 μm samples. In 13–17 μm films shown in Figs. 5(j)–5(l), the N-BE luminescence greatly increases relative to the G band and their intensity ratio seems to approach a constant value. In line with common practice in other semiconductors[36,37] one may take the ratio ρ between the intensities of the G band and the N-BE TO(X) replica as a figure of merit for CVD 3C-SiC films. The relation of the ρ value versus d_{SiC} is shown in Fig. 8. These data are taken from Table V for samples with film thicknesses larger than 4 μm. In Fig. 8, ρ as a function of d_{SiC} is plotted for both the He-Cd laser and the Hg lamp excitation. The shallow 3250-Å exciting radiation shows smaller ρ values than the deeper penetrating Hg excitation.

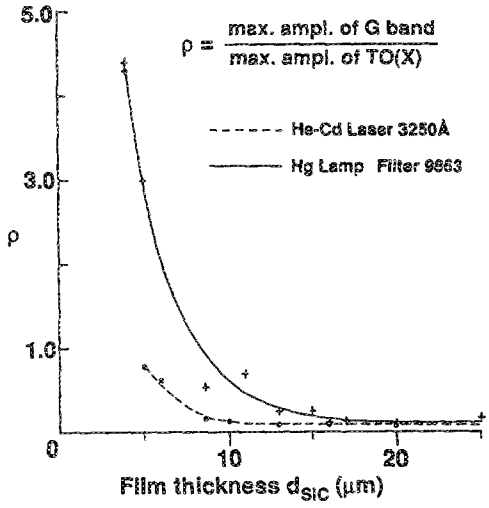

FIG. 8. Intensity ratio ρ as a function of film thickness with two types of optical excitation.

D. D_I line at 1.972 eV

The behavior of the D_I line at 1.972 eV shows some interesting features. As we mentioned already, the D_I line does not appear in samples with d_{SiC} less than 3 μm and sharpens up for d_{SiC} greater than 4 μm. This means that the appearance and sharpness are also, to some extent, an indication of sample perfection. Previously, the D_I line was reported for ion-implanted and electron-irradiated Lely-grown 3C-SiC crystals[27,28] and for as-grown and ion-implanted CVD 3C-SiC films.[25,26] The ion implantation and electron irradiation produces Frenkel pairs and may subsequently form impurity-vacancy complexes, which in turn may be responsible for the recombination radiation from the D_I center. In the CVD samples which we have examined, the interface region consists of a large number of dislocations and other extended defects, and these line defects appear to dominate the observed spectra. For thick films $d_{SiC} > 10\,\mu$m the number of dislocations and extended defects near the surface is considerably reduced and recombination due to point defect complexes appears to become more prominent. Another feature of the D_I line should be pointed out from the data in Table V. Due to the removal of the Si substrate, i.e., a release of the SiC/Si tensile biaxial stress, the D_I line does not shift more than 0.5 meV on either side of the free film. This is to be compared (see Table V) with the large shifts of 4–8 meV that occur upon removal of the tensile stress for the N-BE lines. All of the D_I line positions which we have measured for 3C-SiC with and without Si substrates, including measurements of both sides of the free films, in Figs. 5 and 6 yield D_I line positions that are almost identical. These observations imply that the D_I center is not affected in the same manner by external and internal stresses as the bound-exciton lines. A deep center such as D_I is presumably made up of wave functions from many bands and thus there may be an averaging of the band shifts due to stress and thus a small net shift.

E. Dislocation and extended defect-related G band

Choyke and Patrick[27] have reported the 1.84–1.98-eV PL spectrum of ion-implanted and annealed bulk samples of cubic SiC. They suggested that the observed 66.5 meV side band is a resonant mode shifted to lower energy from the normal LA phonon replica.[27] This 66.5 meV mode is located at 1.907 eV, roughly the same position as the G band, observed in our PL measurements of CVD 3C-SiC films. How-

ever, as can be seen in Fig. 6, the intensity, shape, and lower-energy side bands extending to 1.50 eV are distinctly different from the phonon side band spectrum seen for the D_1 center. We therefore believe the G band and the G_1 and G_2 bands as well as the broad background below 1.75 eV are not related to the D_1 center. We further believe that we have evidence relating them to dislocations and other extended defects. The following experimental facts support this suggestion:

(1) The D_1 line associated with pointlike defects such as a divacancy is not seen in CVD SiC near the interface layer. The G band, on the other hand, is seen in layers close to the interface.

(2) The D_1 lines from different samples have almost the same energy position (1.972 eV) with an error of less than 0.3–0.5 meV, whilst the peak positions of the G band are very different from sample to sample with a shift of up to 10–20 meV. G_1 and G_2 are almost always seen at a constant distance from the G band. Figure 9 shows such an example where the D_1 lines of two samples are located at same position (1.9723 eV) but the two G bands are displaced by ~ 7 meV. If we shift the energy scale for these two samples and align the two G bands then we also find coincidence for the G_1 and G_2 bands. It is possible that G_1 and G_2 in some way are involved with the longitudinal LA(X) and LO(Γ) phonons. But for such a very deep center there is no *a priori* reason to require such momentum conservation.

(3) In Fig. 6 we have the photoluminescence from both sides of a CVD 3C-SiC free film. The top (surface) side which is excited wth 3250-Å light ($1/\alpha \sim 1.5$ μm) shows sharp and strong N-BE lines and relatively weak D_1, G, G_1, and G_2 bands. The bottom (interface) side shows the PL emission from ~ 1.5 μm from the SiC/Si interface. It consists of much weaker N-BE lines and relatively stronger D_1, G, G_1, and G_2 bands indicating a much larger density of line defects in this region. This is consistent with XTEM observations on such films.[11–13] Experimentally, we find the broad background to extend well below 1.50 eV and it may also be related to extended defects which are known to concentrate in this interface region.

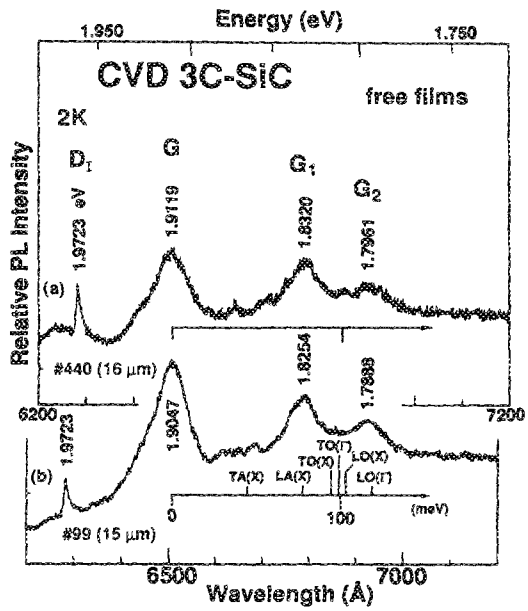

FIG. 9. A comparison of D_1, G, G_1, and G_2 for two CVD 3C-SiC films.

F. Effects of biaxial stress on the relative intensities of BE lines

An interesting phenomenon about the effects of biaxial stress on the relative intensities of N-BE lines is observed by us in this study. For CVD 3C-SiC free films, relieved from the biaxial stress due to the removal of the Si substrate (in Fig. 4), the N-BE zero phonon line N_0 is a strong feature and its intensity is about one tenth that of the dominant TO momentum conserving line. The other one-phonon lines TA, LA, and LO, for the free SiC film No. TP099, have intensity ratios of 0.33, 0.73, and 0.73 with respect to the TO line, as seen in Table VI. However, for CVD samples which have not been removed from the Si substrates, the no-phonon line and the momentum conserving phonons have very different intensity ratios with respect to the TO phonon replica. Not only is the TO line the strongest feature in the N-BE spectrum but it appears to be the only line which does not attenuate appreciably under the influence of the biaxial stress. It is for this reason that we have chosen to take the intensity ratios with respect to the TO line and in this way make comparisons in Table VI between the free SiC film and several stressed films. All spectra were taken under reasonably identical circumstances and the SiC films come from growth runs which were designed to be as similar as possible.

The data in Table VI has considerable scatter but certain trends are apparent:

(1) The no-phonon line is attenuated more than any other line with respect to the free film.

(2) The shift towards lower energy due to the biaxial stress appears to be about 20% less for the no-phonon line than for the phonon replicas.

(3) The intensity of the LA mode appears to be affected most by the biaxial stress, with the LO mode second and the TA mode third. As mentioned previously, the TO mode is hardly affected.

We believe that the intensity changes for the no-phonon line may have a different origin than the intensity changes for the phonon replicas. The no-phonon line is a direct transition and the effect on the band structure at $\mathbf{k} = 0$ due to the biaxial stress could influence the matrix elements for this transition. The slightly reduced energy shift for the no-phonon line due to the stress may be connected with the fact that additional deformation potentials may have to be considered for this transition. In the case of the momentum conserving phonon lines we believe the reduction in intensity with respect to the free film may have its origin in a reduced density of phonon states at the zone boundary. As the symmetry is reduced by the biaxial stress it could be that the requirement which obeys for the zinc-blende lattice, namely, that the lattice modes approach the zone boundary with zero tangent, may not hold. If so, the very flat TO mode would hardly be affected but one might expect substantial changes for the TA, LA, and TO modes. We hope theorists may be

TABLE VI. The intensity ratio of the N-BE lines to the TO phonon lines for CVD 3C-SiC with and without Si substrates. Note: The numbers inside parentheses are the shifts of the line position with respect to that of the free film TP099, in units of meV.

Sample	I_0/I_{TO}	I_{TA}/I_{TO}	I_{LA}/I_{TO}	I_{TO}/I_{TO}	I_{LO}/I_{TO}	d_{SiC} (μm)
TP099	0.14	0.33	0.73	1.0	0.73	15
3C-SiC free film	(0)	(0)	(0)	(0)	(0)	
740-9	0.02	0.16	0.19	1.0	0.30	10.4
3C-SiC/Si (100)	(5.0)	(6.0)	(6.0)	(6.1)	(6.5)	
778-4	0.02	0.16	0.19	1.0	0.32	9.5
3C-SiC/Si (100)	(6.3)	(6.8)	(7.2)	(7.0)	(7.2)	
788-4	0.06	0.18	0.17	1.0	0.22	9.2
3C-SiC/Si (100)	(5.4)	(5.9)	(6.3)	(6.0)	(6.3)	
790-4	0.01	0.1	0.15	1.0	0.19	9.6
3C-SiC/Si (100)	(6.0)	(6.6)	(7.0)	(6.5)	(6.9)	

persuaded to produce calculations so that several of these observations may be checked in a more rigorous fashion.

VI. CONCLUSION

In summary:

(1) A detailed PL study for a series of CVD-grown 3C-SiC thin films on (100) Si substrates with film thicknesses ranging from 600 Å to 25 μm has been performed. The defect-related W band near 2.15 eV and the G band near 1.90–1.92 eV dominate the PL spectra for very thin-film samples. With an increase of d_{SiC} beyond 3 μm, N-BE emission rapidly increases with respect to the G band, while the W band is quenched. Beyond 16 μm the relative intensity ratio between the G band and the N-BE lines approches a constant value suggesting that further improvement in CVD growth of SiC is dependent on the substrate used and the initial nucleation conditions.

(2) 3C-SiC/(100) Si films have been grown by CVD and show a characteristic N-BE spectrum comparable to the one which is found in good bulk crystals grown by the Lely method or from 3C-SiC plates grown from solution. We report well-resolved zero-, one-, and two-phonon lines of N-Be as well as three-phonon replicas. The latter have not previously been reported in the literature.

(3) The D_I band associated with a point-defect complex shows only a very slight change in wavelength when the Si substrate is removed. For thick films (16 μm) its position is unchanged whether the free SiC film is irradiated from the front or the back. This result has been duplicated on numerous samples. It appears that this deep center ($\sim$0.5 eV) is little affected by the internal stresses in the SiC film. This result is consistent with the fact that the wavefunction for a deep level is made up of contributions from many bands in the crystal and is likely to be insensitive to energy shifts of the CB at X and the VB at Γ.

(4) Recombination radiation between 1.50 and 1.95 eV has been examined for a number of conditions of the 3C-SiC film. The G band and its phonon side band G_1 and G_2 are thought to be related to dislocations and extended defects. The 1.5–1.9 eV photoluminescence is likely to be a superposition of the D_I series and the G series, i.e., a mixture of point and extended defects.

(5) The ratio ρ of intensities between the G band and the strongest N-BE line is adopted as an arbitrary figure of merit of crystalline perfection for CVD 3C-SiC films. The near surface region has a much smaller ρ than the interface region. This is consistent with TEM observations showing a high density of dislocations and other defects near the interface. With an increase of d_{SiC} and a decrease of exciting depth, ρ values decrease, indicating a decrease of the density of defects away from the SiC/Si interface.

(6) The effects of stresses on the energy band gap are studied theoretically. General formulas for the band-gap shift due to a generalized axial stress, including the special cases of hydrostatic pressure and uniaxial and biaxial stress, are derived. When applied to the case of the CVD 3C-SiC/Si system, a relation for the deformation potentials of 3C-SiC is obtained. It is shown that beyond the transition layer (1–3 μm), the surface stress decreases slightly and the great release of interface stress and misfit strain is due to the thin transition region.

(7) The effects of biaxial stress on the relative intensities of BE lines are reported. It is observed experimentally that due to the removal of the Si substrate, the intensities of N-BE N_0, TA, LA, and LO lines, with respect to the TO line, become relatively stronger. The biaxial stress in the CVD SiC/Si system depresses the no-phonon line the most with the LA and LO modes next and the TA and TO modes affected least.

ACKNOWLEDGMENTS

This work was supported in part by NASA Grant No. NAG-3-603 and a Grant from the National Science Foundation (DMR84-03596).

[1]J. A. Powell, L. G. Matus, and M. A. Kuczmarski, J. Electrochem. Soc. 134, 1558 (1987).

[2]S. Nishino, H. Suhara, H. Ono, and H. Matsunami, J. Appl. Phys. **61**, 4889 (1987).
[3]J. Lely, Ber. Dtsch. Keram. Ges. **32**, 229 (1955).
[4]S. Nishino, J. A. Powell, and H. A. Will, Appl. Phys. Lett. **42**, 460 (1983).
[5]A. Addamiano and J. A. Sprague, Appl. Phys. Lett. **44**, 525 (1984).
[6]K. Sasaki, E. Sakuma, S. Misawa, S. Yoshida, and S. Gonda, Appl. Phys. Lett. **45**, 72 (1984).
[7]P. Liaw and R. F. Davis, J. Electrochem. Soc. **132**, 642 (1985).
[8]P. Liaw and R. F. Davis, J. Electrochem. Soc. **131**, 3014 (1984).
[9]Z. C. Feng, A. Mascarenhas, W. J. Choyke, and J. A. Powell, J. Appl. Phys. **64**, 3176 (1988).
[10]Z. C. Feng, W. J. Choyke and J. A. Powell (unpublished).
[11]C. H. Carter, Jr., J. A. Edmond, J. W. Palmour, J. Ryu, H. J. Kim, and R. F. Davis, Mater. Res. Soc. Symp. Proc. **46**, 593 (1985).
[12]S. R. Nutt, D. J. Smith, H. J. Kim, and R. F. Davis, Appl. Phys. Lett. **50**, 203 (1987).
[13]P. Pirouz, C. M. Chorey, and J. A. Powell, Appl. Phys. Lett. **50**, 221 (1987).
[14]G. E. Picus and G. L. Bir, Sov. Phys.—Solid State **1**, 136 (1959); **1**, 1502 (1960).
[15]W. H. Kleiner and L. M. Roth, Phys. Rev. Lett. **2**, 334 (1959).
[16]F. H. Pollak and M. Cardona, Phys. Rev. **172**, 816 (1968).
[17]F. H. Pollak, Surf. Sci. **37**, 863 (1973).
[18]H. D. Liu and Z. C. Feng, IEEE J. Quantum Electron. **QE-19**, 1016 (1983).
[19]H. Asai and K. Oe, J. Appl. Phys. **54**, 2052 (1983).
[20]C. P. Kuo, S. K. Vong, R. M. Cohen, and G. B. Stringfellow, J. Appl. Phys. **57**, 5428 (1985).
[21]Z. C. Feng, Ph.D. thesis, University of Pittsburgh, 1987.
[22]W. J. Choyke, D. R. Hamilton, and L. Patrick, Phys. Rev. **133**, A1163 (1964).
[23]R. L. Hartman and P. J. Dean, Phys. Rev. B **2**, 951 (1970).
[24]P. J. Dean, W. J. Choyke, and L. Patrick, J. Lumin. **15**, 299 (1977).
[25]J. A. Freitas, Jr., S. G. Bishop, A. Addamiano, P. H. Klein, H. J. Kim, and R. F. Davis, Mater. Res. Soc. Proc. **46**, 581 (1985).
[26]K. A. Freitas, Jr., S. G. Bishop, J. A. Edmond, J. Ryu, and R. F. Davis, J. Appl. Phys. **61**, 2011 (1987).
[27]W. J. Choyke and L. Patrick, Phys. Rev. B **4**, 1843 (1971).
[28]W. J. Choyke, in *Radiation Effects in Semiconductors, 1976,* edited by N. B. Urli and J. W. Corbet, Inst. Phys. Conf. Ser. No. 31 (Institute of Physics, London, 1977), p. 58.
[29]Z. C. Feng, A. Mascarenhas, W. J. Choyke, and J. A. Powell, Bull. Am. Phys. Soc. **31**, 351 (1986).
[30]H. Mukaida, H. Okumura, J. H. Lee, H. Daimon, E. Sakuma, K. Endo, and S. Yoshida, J. Appl. Phys. **62**, 254 (1987).
[31]G. A. Slack, J. Appl. Phys. **35**, 3460 (1964).
[32]S. Ganesan, A. A. Maradudin, and J. Oitmaa, Ann. Phys. **56**, 556 (1970).
[33]R. G. Humphreys, D. Bimberg, and W. J. Choyke, Solid State Commun. **39**, 163 (1981).
[34]I. S. Gorban', V. A. Kravets, G. N. Mishionova, and K. V. Nazarenko, Sov. Phys. Semicond. **10** 1254 (1976).
[35]L. Patrick and W. J. Choyke, J. Phys. Chem. Solids **34**, 565 (1973).
[36]Z. C. Feng, A. Mascarenhas, W. J. Choyke, R. F. C. Farrow, F. A. Shirland, and W. J. Takei, Appl. Phys. Lett. **47**, 24 (1985).
[37]Z. C. Feng, A. Mascarenhas, and W. J. Choyke, J. Lumin. **35**, 329 (1986).